Body-wave radiation patterns and AVO in transversely isotropic media

Ilya Tsvankin*

ABSTRACT

The angular dependence of reflection coefficients may be significantly distorted in the presence of elastic anisotropy. However, the influence of anisotropy on amplitude variation with offset (AVO) analysis is not limited to reflection coefficients. AVO signatures (e.g., AVO gradient) in anisotropic media are also distorted by the redistribution of energy along the wavefront of the wave traveling down to the reflector and back up to the surface. Significant anisotropy above the target horizon may be rather typical of sand-shale sequences commonly encountered in AVO analysis.

Here, I examine the influence of P- and S-wave radiation patterns on AVO in the most common anisotropic model—transversely isotropic media. A concise analytic solution, obtained in the weak-anisotropy approximation, provides a convenient way to estimate the impact of the distortions of the radiation patterns on AVO results. It is shown that the shape of the P-wave radiation pattern in the range of angles most

important to AVO analysis (0–40°) is primarily dependent on the *difference* between Thomsen parameters ε and δ. For media with $\varepsilon - \delta > 0$ (the most common case), the P-wave amplitude may drop substantially over the first 25–40° from vertical. There is no simple correlation between the strength of velocity anisotropy and angular amplitude variations. For instance, for models with a fixed positive $\varepsilon - \delta$ the amplitude distortions are less pronounced for larger values of ε and δ. The distortions of the SV-wave radiation pattern are usually much more significant than those for the P-wave.

The anisotropic directivity factor for the incident wave may be of equal or greater importance for AVO than the influence of anisotropy on the reflection coefficient. Therefore, interpretation of AVO anomalies in the presence of anisotropy requires an integrated approach that takes into account not only the reflection coefficient but also the wave propagation above the reflector.

INTRODUCTION

Amplitude variation with offset (AVO) analysis is one of the few exploration methods that is used widely for the direct detection of hydrocarbons. Conventional AVO algorithms are based on analytic expressions for the plane P-wave reflection coefficient for isotropic media. The presence of elastic anisotropy on either side of the reflector may significantly distort the angular dependence of reflection coefficients (e.g., Keith and Crampin, 1977; Banik, 1987; Wright, 1987; Graebner, 1992). Banik (1987) and Thomsen (1993) developed analytic approximations for the reflection coefficient at a boundary between two transversely isotropic

media in the limit of weak anisotropy and of small velocity and density contrasts across the reflector. A numerical analysis of the P-wave[1] reflection coefficient at the interface between anisotropic shales and isotropic gas sands was given in Kim et al. (1993). Blangy (1994) presented an overview of the influence of transverse isotropy on the P-wave reflection coefficient. Yet another substantial distortion of the AVO signature in anisotropic media is associated with the wave propagation above the reflector.

The real goal of AVO is to perform reflection coefficient-versus-angle analysis rather than directly studying the amplitude variation with offset. Hence, correction for the

[1] The qualifiers in "quasi-P-wave" and "quasi-SV-wave" will be omitted for brevity.

angular amplitude variation caused by the wave phenomena above the reflector is an essential component of AVO technology. Propagation effects, usually described in the ray approximation, include source directivity, energy divergence, and transmission and attenuation losses along the raypath (Duren, 1992). Although correction for propagation phenomena in realistic inhomogeneous subsurface models encounters many practical difficulties (Martinez, 1993), it is well understood if the medium is isotropic.

If the velocity above the reflector is angle-dependent, the behavior of body-wave amplitudes becomes much more complicated, and the isotropic correction becomes inadequate. The presence of anisotropic layers above the target horizon may be quite typical for sand-shale sequences commonly considered in AVO analysis (Kim et al., 1993). While reservoir sands can be expected to exhibit very weak anisotropy (if any), shale formations are often characterized by strong transverse isotropy, i.e., pronounced velocity variations in the incidence (vertical) plane (White et al., 1983; Robertson and Corrigan, 1983; Banik, 1984; Sams et al., 1993, among others).

A systematic description of point-source radiation patterns in transversely isotropic and orthorhombic media was given in Tsvankin and Chesnokov (1990a). Along with numerical analysis based on evaluation of Fourier-Bessel integrals, Tsvankin and Chesnokov presented an analytic solution for radiation patterns derived from the stationary-phase approximation. Their results showed that the distribution of energy along wavefronts in anisotropic media is substantially distorted by focusing and defocusing of energy, usually associated with maxima and minima, respectively, in the angle-dependent velocity.

Asymptotic ray-theory expressions for radiation patterns in anisotropic media have been derived by Ben-Menahem et al. (1991) and Gajewski (1993). Gajewski (1993) developed an efficient numerical scheme to evaluate the Gaussian curvature of the slowness surface needed to calculate radiation patterns and gave a detailed discussion of body-wave amplitudes in models containing aligned liquid-filled and dry cracks. A numerical example illustrating the influence of the distortion of P-wave radiation patterns on AVO was presented in Samec and Blangy (1992).

The main goal of this paper is to study the influence of the distortions of body-wave radiation patterns in transversely isotropic media on AVO analysis. The existing solutions for point-source radiation in anisotropic models require numerical evaluation and do not provide easy analytic insight into the problem. Here, I present a concise weak-anisotropy approximation for radiation patterns in transversely isotropic media that relates the distortions of point-source radiation to the Thomsen parameters ε, δ (for the P- and SV-wave) and γ (for the SH-wave). The weak-anisotropy solution is compared with results of exact numerical modeling and with the stationary-phase approximation developed in Tsvankin and Chesnokov (1990a). Analysis of radiation patterns in the range of angles most important for AVO (0–40°) is followed by a comparison of the influence of transverse isotropy on two principal components of the AVO signature—the wave propagation above the reflector and the reflection coefficients.

GENERAL ANALYSIS FOR TRANSVERSE ISOTROPY

Far-field point-source radiation in isotropic homogeneous, nonattenuating media is determined just by the source directivity factor and the spherical divergence of amplitude (Aki and Richards, 1980). The far-field approximation for source radiation in anisotropic media, derived in Tsvankin and Chesnokov (1990a) by means of the stationary-phase method, is a much more complicated function that depends on the shape of the slowness surface. The most significant distortion of radiation patterns in anisotropic media is caused by the phenomena defined by Tsvankin and Chesnokov as "focusing" and "defocusing" of energy. Energy increases (focuses) in parts of the wavefront with a high concentration of group-velocity vectors of elementary plane waves (which comprise point-source radiation). Conversely, defocusing corresponds to areas with a low concentration of group-velocity vectors. Often (but not always) focusing takes place near velocity maxima, while defocusing is often associated with velocity minima.

Quantitative analysis of radiation patterns in Tsvankin and Chesnokov (1990a) was performed by a numerical technique based on plane-wave decomposition of point-source radiation with subsequent evaluation of Fourier-Bessel integrals in the frequency domain. In contrast with the exact (but more time-consuming) method in Fryer and Frazer (1987), the algorithm introduced by Tsvankin and Chesnokov involves an approximate treatment of azimuthal anisotropy; however, it is exact for azimuthally isotropic media. The stationary-phase approximation was used by them only for qualitative estimates. Here, the stationary-phase solution for radiation patterns is transformed into a much simpler expression valid for weak transverse isotropy.

I consider a simple model of a horizontal reflector below a transversely isotropic medium with a vertical symmetry axis (VTI) (Figure 1). Transverse isotropy will be described by the vertical velocities V_{P0} and V_{S0} of P- and S-waves, respectively, and three dimensionless anisotropic parameters ε, δ, and γ introduced in Thomsen (1986):

$$\varepsilon \equiv \frac{c_{11} - c_{33}}{2c_{33}}, \tag{1}$$
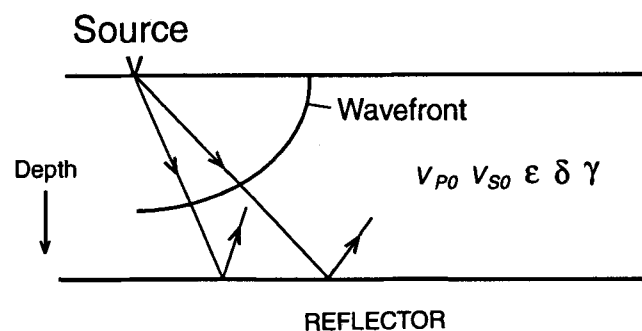
Source

FIG. 1. Reflection from the bottom of a transversely isotropic layer. Anisotropy distorts the angular amplitude distribution of the incident wave.

$$\delta \equiv \frac{(c_{13} + c_{44})^2 - (c_{33} - c_{44})^2}{2c_{33}(c_{33} - c_{44})}, \qquad (2)$$

$$\gamma \equiv \frac{c_{66} - c_{44}}{2c_{44}}, \qquad (3)$$

where c_{ij} are stiffness coefficients.

Although originally designed for weakly anisotropic models, the parameters ε, δ, and γ are convenient to use in TI media with arbitrarily strong velocity anisotropy (Tsvankin and Thomsen, 1994). P-SV propagation is described by the parameters V_{P0}, V_{S0}, ε, and δ, while the SH-wave velocity depends on V_{S0} and γ (SH-wave anisotropy is elliptical).

The influence of the free surface on radiation patterns is not taken into account, nor is that of source and receiver arrays. Here I concentrate only on the propagation phenomena caused by velocity anisotropy. These anisotropy-induced distortions of wavefront amplitudes are quite general since they take place not only in the source layer but in any other anisotropic layer encountered by the ray. The pure influence of the wavefront-focusing phenomena is also of prime interest in crosshole and reverse VSP surveys that employ buried sources.

It is important to mention that the radiation patterns in this paper are derived as a function of the phase or group angle with the symmetry axis; therefore, the analytic developments below apply not only for VTI media but also for transverse isotropy with any orientation of the axis of symmetry.

Derivation of the weak-anisotropy approximation for point-source radiation is given in the Appendix. The far-field radiation pattern of P, SV, or SH-waves from a point force for weak transverse isotropy ($|\varepsilon| \ll 1$, $|\delta| \ll 1$, $|\gamma| \ll 1$) is shown to be

$$U(R, \theta) = \frac{F_u}{4\pi\rho V^2(\theta)R} \frac{1}{\sqrt{\frac{\sin \psi}{\sin \theta}\left(1 + \frac{1}{V}\frac{d^2V}{d\theta^2}\right)}}, \qquad (4)$$

where U is the magnitude of the displacement, θ is the phase angle measured from the symmetry axis, V is the phase velocity, ρ is the density, and $R = \sqrt{z^2 + r^2}$ (z is the receiver depth with r being the horizontal source-receiver offset). The source term F_u is the projection of the force on the displacement (polarization) vector. Expression (4) should be evaluated at the phase angle θ, corresponding to a given ray (group-velocity) angle $\psi = \tan^{-1}(r/z)$ of the incident wave. It can be shown that at velocity maxima or minima the phase and group velocity vectors coincide with each other.

Equation (4) demonstrates how point-source radiation is distorted by velocity anisotropy. Although the term $F_u/(4\pi\rho V^2 R)$ formally coincides with the well-known expression for the far-field, point-force radiation in isotropic media (Aki and Richards, 1980), the phase velocity in equation (4) is angle-dependent. Since body-wave polarizations depend on the elastic constants (e.g., for the P-wave the polarization vector deviates from the ray), the source term F_u may also be distorted by the anisotropy. Also, the expression should

be evaluated in the phase direction (angle θ), which is generally different from the source-receiver direction because of the presence of anisotropy. The term under the radical represents the pure contribution of the anisotropy to the radiation pattern. As shown in Tsvankin and Chesnokov (1990a), the second derivative of phase velocity is responsible for the focusing and defocusing phenomena mentioned above.

The distinction between the source term F_u and the rest of equation (4) is very important. While F_u is itself distorted by the anisotropy, the existence of the remaining anisotropic terms means that the redistribution of energy along the wavefront happens not only in the source layer but also in any other anisotropic layer along the raypath.

Linearization of equation (4) in terms of the anisotropy parameters ε, δ, and γ leads to concise expressions for the P-, SV- and SH-waves that provide analytic insight into the amplitude distortions in transversely isotropic media.

P-WAVE RADIATION PATTERNS

Weak-anisotropy approximation for P-wave radiation

The issue of P-wave AVO is of particular importance because P-waves constitute the overwhelming majority of all seismic data being used in exploration. The P-wave phase-velocity function for weak transverse isotropy ($|\delta| \ll 1$, $|\varepsilon| \ll 1$), fully linearized in ε and δ, is given by (Thomsen, 1986)

$$V_P(\theta) = V_{P0}(1 + \delta \sin^2 \theta \cos^2 \theta + \varepsilon \sin^4 \theta). \qquad (5)$$

Differentiating equation (5) twice with respect to the phase angle θ yields

$$\frac{d^2[V_P(\theta)]}{d\theta^2} = 2V_{P0}[\delta \cos 4\theta + 2\varepsilon \sin^2 \theta(1 + 2 \cos 2\theta)]. \qquad (6)$$

Also, for weak anisotropy (see Thomsen, 1986)

$$\sin \psi = \sin \theta\{1 + \cos^2 \theta[2\delta + 4(\varepsilon - \delta) \sin^2 \theta]\}. \qquad (7)$$

Substituting the above equations into equation (4), applying a Taylor series expansion, and dropping the terms quadratic in δ and ε, we obtain the weak-anisotropy approximation for the P-wave radiation pattern,

$$U_P(R, \theta) = \frac{F_u}{4\pi\rho V_{P0}^2 R} \frac{1 - 2(\varepsilon - \delta) \sin^2 2\theta + \delta \sin^2 \theta}{1 + 2\delta}. \qquad (8)$$

The term $1 + 2\delta$ has been retained in the denominator to make the weak-anisotropy approximation exact in the symmetry direction ($\theta = 0$). [By using formula (A-4), it can be shown that the exact far-field P-wave amplitude in the symmetry direction is given by $F_3/[4\pi\rho V_{P0}^2 R(1 + 2\delta)]$, where F_3 is the vertical component of the force.] Equation (8) may produce errors at oblique incidence if ε and δ are not small.

Note that $V_{P0}^2(1 + 2\delta)$ is equal to the squared P-wave normal-moveout (NMO) velocity from a horizontal reflector. This means that the influence of transverse isotropy on the amplitude in the symmetry direction and on the NMO velocity is determined by the same expression: $1 + 2\delta$.

Thus, the focusing (or defocusing) of the P-wave energy at vertical incidence depends on the single anisotropic coefficient δ, the parameter responsible for near-vertical P-wave propagation. If $\delta < 0$, the velocity function has a maximum at $\theta = 0°$, and the amplitude at vertical incidence increases as a result of the focusing of energy. Conversely, if $\delta > 0$, a velocity minimum leads to lower amplitudes at $\theta = 0°$ because of the defocusing. It should be emphasized that the velocity maximum or minimum in the symmetry direction represents the only "3-D" velocity extremum in transversely isotropic media: phase velocity increases (or decreases) away from the symmetry axis in all directions, not just in the incidence plane. Therefore, the focusing (or defocusing) of energy in the symmetry direction is more pronounced than that for any other velocity extremum with the same value of $d^2V/d\theta^2$. This peculiarity of the symmetry direction is reflected in equation (4) by the value of the ratio $\sin\psi/\sin\theta$ at $\psi = \theta = 0$ [equation (7)]:

$$\lim_{\theta \to 0} \frac{\sin\psi}{\sin\theta} = 1 + 2\delta,$$

whereas $\sin\psi/\sin\theta = 1$ at any other velocity extremum.

While distortions of absolute amplitude are diagnostic of anisotropy, the property of radiation patterns of most importance in AVO analysis is the anisotropic correction to the angular amplitude distribution. The lowest-order anisotropic angular term in equation (8) depends on the difference $\varepsilon - \delta$ (more exactly, at small angles the angular amplitude variation is determined by $8\varepsilon - 9\delta$). If $\varepsilon - \delta > 0$ (the most common case in crustal rocks), transverse isotropy causes the P-wave amplitude to decrease away from vertical. For elliptical anisotropy ($\varepsilon = \delta$), the term $2(\varepsilon - \delta)\sin^2 2\theta$ vanishes, and the anisotropic angular correction reduces to $\delta \sin^2 \theta$. This means that for elliptical anisotropy P-wave angular amplitude and velocity variations [see equation (5)] correlate with each other because both depend on δ in a similar fashion. However, the magnitude of the anisotropy-induced angular correction (given by $\delta \sin^2 \theta$) between 0 and 40° is relatively small unless δ is unusually large. Finally, if $\varepsilon - \delta < 0$ we can expect an increase in the P-wave amplitude with angle because of transverse isotropy.

Angular distortions of the radiation pattern may also be caused by the source term F_u, which depends on the polarization vector. As shown by Tsvankin ("P-wave signatures and notation for transversely isotropic media: An overview," accepted for publication in GEOPHYSICS, 1996), in the weak-anisotropy approximation the P-wave polarization angle ϕ (measured from the symmetry axis) is given by

$$\tan\phi = \tan\theta\{1 + B[2\delta + 4(\varepsilon - \delta)\sin^2\theta]\}, \quad (9)$$

$$B = \frac{1}{2(1 - V_{S0}^2/V_{P0}^2)}.$$

An analysis of equation (9) [compare with equation (A-20) for the group angle] and the numerical study in Tsvankin and Chesnokov (1990a), show that for moderate velocity anisotropy, the P-wave polarization vector does not diverge much from the group (ray) direction. This means that the source term F_u for the P-wave is almost "isotropic," i.e., for a unit force it is close to the absolute value of the cosine of the

angle between the force and the group-velocity vector. For moderate anisotropies $|\varepsilon| \leq 0.2$, $|\delta| \leq 0.2$, the distortions of the point-force directivity factor F_u in the angular range 0–40° are limited to a few percent. For other sources, such as dislocations or explosions, the dependence of the source term on anisotropy is more complicated and can make a more significant contribution to the distortions of the angular amplitude distribution (Tsvankin and Chesnokov, 1990b).

It is more convenient to represent radiation patterns as a function of the group angle ψ that determines the source-receiver direction ($\psi = \tan^{-1}(r/z)$). Formally, the difference between the phase and group angles for the terms $2(\varepsilon - \delta)\sin^2 2\theta$ and $\delta \sin^2 \theta$ in equation (8) can simply be ignored. If we replace θ in formula (8) by the group angle ψ [using equation (7)] and do linearization in ε and δ, we get exactly the same expression (8) but with the group angle in place of the phase angle. Nevertheless, when the absolute values of the anisotropies approach 15–20%, the accuracy of the weak-anisotropy approximation is increased by evaluating expression (8) at the phase angle corresponding to a given group angle.
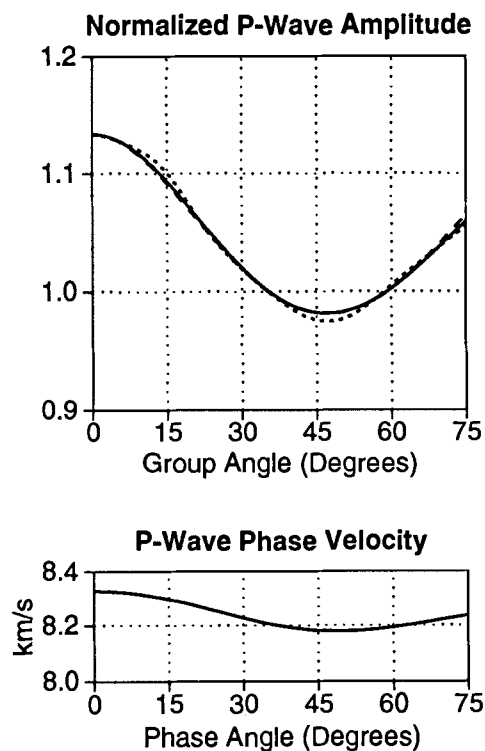

FIG. 2. P-wave amplitude from a point vertical force in transversely isotropic olivine ($V_{P0} = 8.328$ km/s, $V_{S0} = 4.606$ km/s, $\varepsilon = -0.008$, $\delta = -0.059$). The dotted curve is the exact result obtained by evaluating Fourier-Bessel integrals; the solid curve is the stationary-phase solution (A-4); and the dashed curve is the weak-anisotropy approximation (8). All curves are normalized by the radiation pattern in the corresponding isotropic medium ($\varepsilon = 0$, $\delta = 0$). The phase-velocity curve is shown at the bottom. The receiver is located at a constant distance R from the source in the far-field ($R/\lambda_p \approx 12$, where λ_p is the average P-wavelength in the isotropy plane).

Analysis of far-field P-wave amplitudes

I begin by discussing the amplitude signature for the olivine model considered in Tsvankin and Chesnokov (1990a) and proceed with a systematic analysis for a suite of transversely isotropic models parameterized by ε and δ. Figure 2 shows the P-wave amplitudes excited by a point vertical force for transversely isotropic olivine with $\varepsilon - \delta = 0.051$. The dotted curve in Figure 2 is the exact result obtained by evaluating Fourier-Bessel integrals as described in Tsvankin and Chesnokov (1990a); the solid curve is the stationary-phase solution, equation (A-4), valid in the far-field for arbitrary strength of the anisotropy; and the dashed curve is the far-field, weak-anisotropy approximation (8) (it can hardly be distinguished from the solid curve). The weak-anisotropy result was calculated using equations (7) and (9) for the group and polarization angles, respectively.

To demonstrate the influence of anisotropy, all three curves in Figure 2 are normalized by the radiation pattern for the corresponding isotropic medium ($\varepsilon = 0$, $\delta = 0$), given as $\cos \psi/(4\pi\rho V_{P0}^2 R)$ (for a unit force). In addition to revealing the angular distortions, this correction makes it possible to see the difference in the absolute amplitude caused by the anisotropy.

For the olivine model in Figure 2, transverse isotropy leads to a decrease in amplitude away from vertical down to a minimum near 45–50°. At a group angle of 45°, the exact

normalized amplitude (dotted curve) is 14% lower than that at vertical incidence. Note that the P-wave phase velocity has a maximum at $\theta = 0°$ and a minimum near $\theta = 49°$. Thus, the decrease in the P-wave amplitude is caused by the focusing of energy at vertical incidence and defocusing near 45–50°. Although a distortion of 14% over a 45° interval does not seem to be significant, it occurs in a medium with less than 2% maximum variation in the P-wave phase velocity!

The stationary-phase result (A-4) diverges from the exact amplitude only in the vicinity of the minimum of the radiation pattern (located at $\psi = 90°$, not shown in Figure 2) because of the nongeometrical effects described in Tsvankin and Chesnokov (1990a). The values of ε and δ for transversely isotropic olivine are small and, predictably, the accuracy of the weak-anisotropy approximation is high.

Before proceeding with the P-wave amplitude analysis for a range of TI models, it is necessary to find out what parameters have an impact on P-wave radiation. Clearly, the influence of transverse isotropy on P-wave amplitudes is mostly determined by the anisotropy parameters ε and δ. However, the P-wave radiation pattern also depends on the vertical velocities V_{P0} and V_{S0}. While the P-wave velocity V_{P0} is just a scaling coefficient that does not change the shape of the radiation pattern (for constant ε, δ, and V_{P0}/V_{S0}), the contribution of the S-wave velocity V_{S0} to the P-wave amplitude needs to be evaluated.
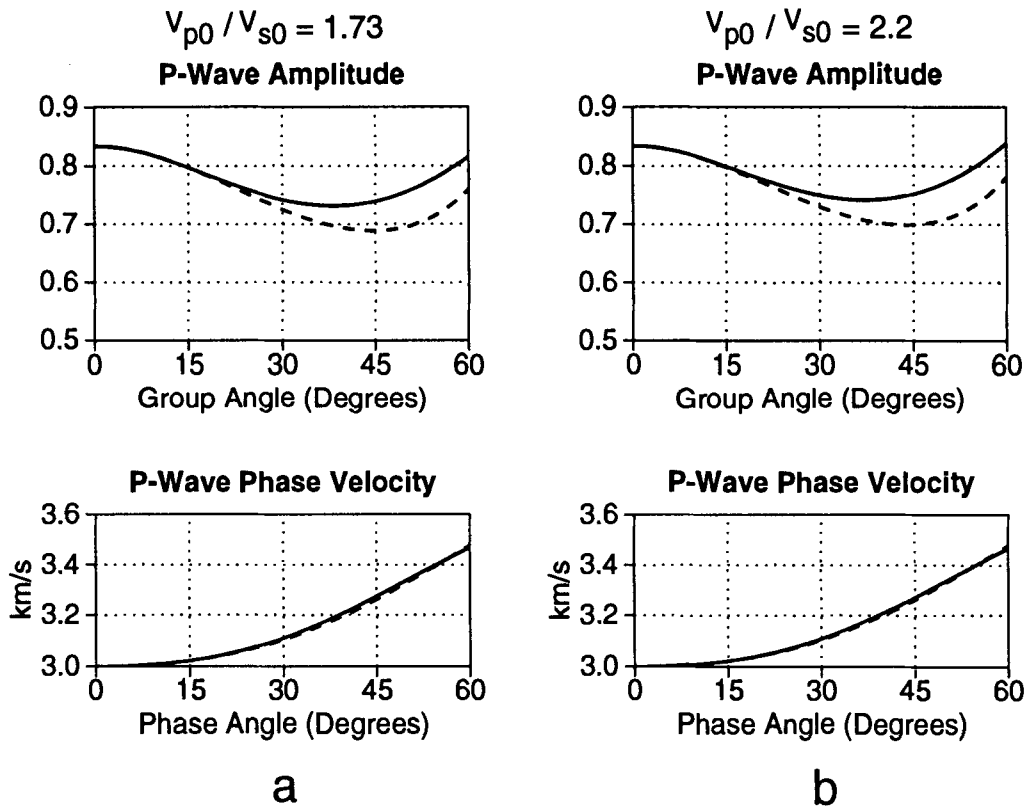

FIG. 3. The influence of the S-wave vertical velocity on P-wave amplitudes from a vertical force for the model with $\varepsilon = 0.25$, $\delta = 0.1$, and $V_{P0} = 3$ km/s. The solid curve is the stationary-phase solution (A-4); the dashed curve is the weak-anisotropy approximation (8). The amplitude curves are normalized by the radiation pattern in the corresponding isotropic model ($\varepsilon = 0$, $\delta = 0$). The plots at the bottom show the exact phase velocity (solid curve) and its weak-anisotropy approximation (5) (dashed curve).

Tsvankin and Thomsen (1994) showed that if a TI medium is parameterized by V_{P0}, V_{S0}, ε and δ, the influence of the S-wave vertical velocity on P-wave traveltimes is practically negligible, even for strong anisotropy. The situation with the amplitudes looks more complicated. Although there is no explicit dependence on V_{S0} in the weak-anisotropy approximation (8), the source term F_u is somewhat dependent on V_{S0} through the polarization direction [equation (9)]. The influence of V_{S0} on the stationary-phase solution [equation (A-4)] is expected to be stronger because several components of the Christoffel tensor in equation (A-4) contain the elastic coefficient c_{44} and, consequently, the velocity V_{S0} (see Appendix).

However, as illustrated by Figure 3, not only the velocity but also the far-field amplitude of the P-wave is practically independent of the S-wave vertical velocity. For a V_{P0}/V_{S0} ratio varying from 1.73 (a) to 2.2 (b), the exact far-field amplitude in the 0–40° angular range changes by less than 1.5%. In the suite of plots starting with Figure 3, I show P-wave radiation patterns from a vertical (parallel to the symmetry axis) force calculated using the stationary-phase expression (A-4) (solid curve) and the weak-anisotropy approximation (8) (dashed curve). As in Figure 2, both curves are normalized by the radiation pattern in the corresponding isotropic medium ($\varepsilon = 0$, $\delta = 0$). The exact phase velocity (solid curve) and its weak-anisotropy approximation (5) (dashed curve) are shown at the bottom.

Now, I continue with a discussion of P-wave amplitude signatures for a representative set of transversely isotropic models. The olivine model in Figure 2 is a weakly anisotropic medium with small negative $\delta(-0.059)$ and $\varepsilon \approx 0$. While both positive and negative values of δ are plausible, ε is almost always positive (Thomsen, 1986). With decreasing δ and increasing ε ($\varepsilon > 0$, $\delta < 0$), the second derivative of the velocity function [equation (6)] increases more rapidly with angle. Consequently, the defocusing of energy away from vertical [equation (4)] becomes more pronounced and spreads over a wider range of angles. It is important to mention that the maximum energy defocusing in this case is shifted from the velocity minimum towards larger angles because $d^2 V_P/d\theta^2$ continues to increase even beyond the velocity minimum. In equation (8), this defocusing trend manifests itself through the behavior of the two anisotropic angular terms.

Therefore, for more typical weakly anisotropic models with $\delta < 0$, $\varepsilon > 0$ ($|\delta| \leq 0.1$, $|\varepsilon| \leq 0.1$), the P-wave amplitude may drop by 20–30% and more between 0 and 40° (Figure 4a). Note that there is no direct correlation between the P-wave amplitude anomalies in the 0–40° range and the shape of the phase-velocity function. Figure 4 also shows that the P-wave radiation pattern is controlled more by the difference $\varepsilon - \delta$ than by the individual values of the anisotropic coefficients.

According to the existing measurements made at seismic frequencies, typically $\varepsilon > \delta$ (Thomsen, 1986; Tsvankin and Thomsen, 1994). For instance, ε is always greater than δ for transversely isotropic media formed by thin bedding of isotropic layers (Berryman, 1979). Thus, decrease in amplitude with angle may be typical for P-wave propagation through transversely isotropic subsurface formations such as shales.

In spite of the apparent similarity, there is a certain difference between the P-wave amplitude signatures for the

two models with $\varepsilon - \delta = 0.1$ in Figure 4. First, the anisotropy leads to a higher amplitude at vertical incidence in Figure 4a because of the focusing/defocusing phenomena near vertical, discussed above. Second, in agreement with the weak-anisotropy approximation (8), the angular amplitude variations (that are of primary interest to us in this problem) are milder for the model with a larger value of δ (Figure 4b).

The angular dependence of P-wave amplitudes for two media with a larger positive $\varepsilon - \delta = 0.2$ is shown in Figure 5. As predicted by the weak-anisotropy approximation, the influence of the anisotropy on the P-wave amplitude becomes more pronounced with increasing $\varepsilon - \delta$. For the model in Figure 5a, which is still formally considered weakly anisotropic, the drop in the normalized amplitude (using the solid curve) from 0 to 40° reaches 35%! For the model in Figure 5b, despite a much larger value of ε and more significant phase-velocity variations, the amplitude distortions are more moderate (about 21%).

As illustrated by this example, the terms "weak anisotropy" or "strong anisotropy" are meaningless without reference to a particular problem. While the model with $\varepsilon = 0.1$, $\delta = -0.1$ is weakly anisotropic in terms of velocity variations, it qualifies as strongly anisotropic in terms of P-wave amplitude distortions. Different seismic phenomena (e.g., group velocities, normal moveout velocities, dip-moveout signatures, amplitudes, etc.) depend on different combinations of anisotropic coefficients. These effective parameters are not easy to infer from the exact solutions. The power of the weak-anisotropy approximation is in providing a convenient tool for developing analytic insight into the influence of anisotropy on wave propagation.

While the weak-anisotropy approximation gives a valid qualitative description of the amplitude anomalies, it deviates from the exact solution with increasing $|\varepsilon|$ and $|\delta|$, as well as with increasing angle. For the model with $\varepsilon = 0.25$, $\delta = 0.05$, the exact amplitude at a group angle of 40° is about 10% higher than the weak-anisotropy result. Although this error cannot be considered as large given the value of ε, it may still look surprising, because the weak-anisotropy phase-velocity curve in the 0–60° range is close to the exact one (Figure 5). However, we should keep in mind that while deriving the weak-anisotropy expression (8), we have linearized in ε and δ not only the phase velocity itself, but also its two derivatives, the group-velocity angle, the expression for $|U_{p\ell}|$ containing the components of the Christoffel matrix (see the Appendix), and the fraction in equation (4). This multiple linearization may lead to much higher errors in the weak-anisotropy approximation for amplitude than those in the linearized phase-velocity function.

Next, I consider elliptical anisotropy—a special case of transverse isotropy that occurs if $\varepsilon = \delta$. For elliptical anisotropy the stationary-phase solution reduces to a simple function of the group angle ψ without application of the weak-anisotropy approximation

$$U_P(elliptical) = \frac{F_u}{4\pi\rho V_{P0}^2 R} \frac{1}{\sqrt{(1 + 2\delta)(1 + 2\delta \cos^2 \psi)}}.$$

(10)

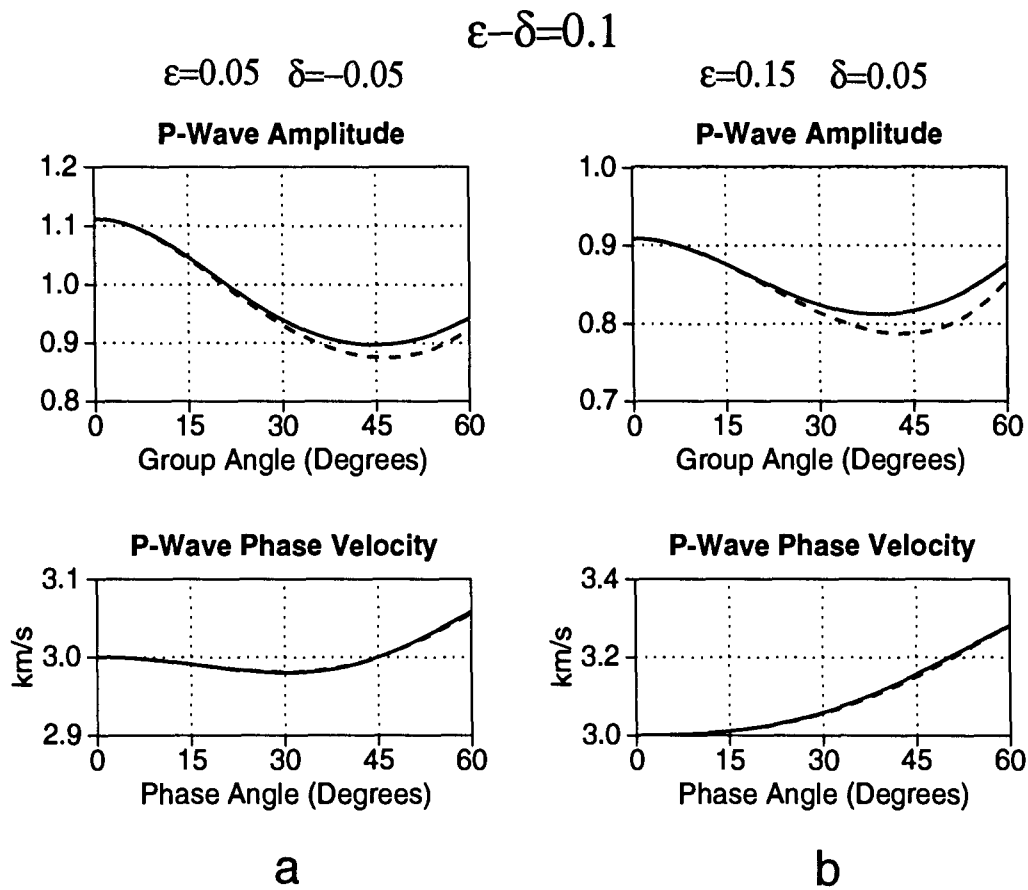As discussed above, the influence of anisotropy on the P-wave radiation patterns in elliptically-anisotropic models

ε–δ=0.1

ε=0.05   δ=−0.05

P-Wave Amplitude

Group Angle (Degrees)

P-Wave Phase Velocity

km/s

Phase Angle (Degrees)

a

ε=0.15   δ=0.05

P-Wave Amplitude

Group Angle (Degrees)

P-Wave Phase Velocity

km/s

Phase Angle (Degrees)

b

FIG. 4. Normalized P-wave amplitude from a vertical force for two models with the same ε − δ = 0.1.

ε–δ=0.2

ε=0.1   δ=−0.1

P-Wave Amplitude

Group Angle (Degrees)

P-Wave Phase Velocity

km/s

Phase Angle (Degrees)

a

ε=0.25   δ=0.05

P-Wave Amplitude

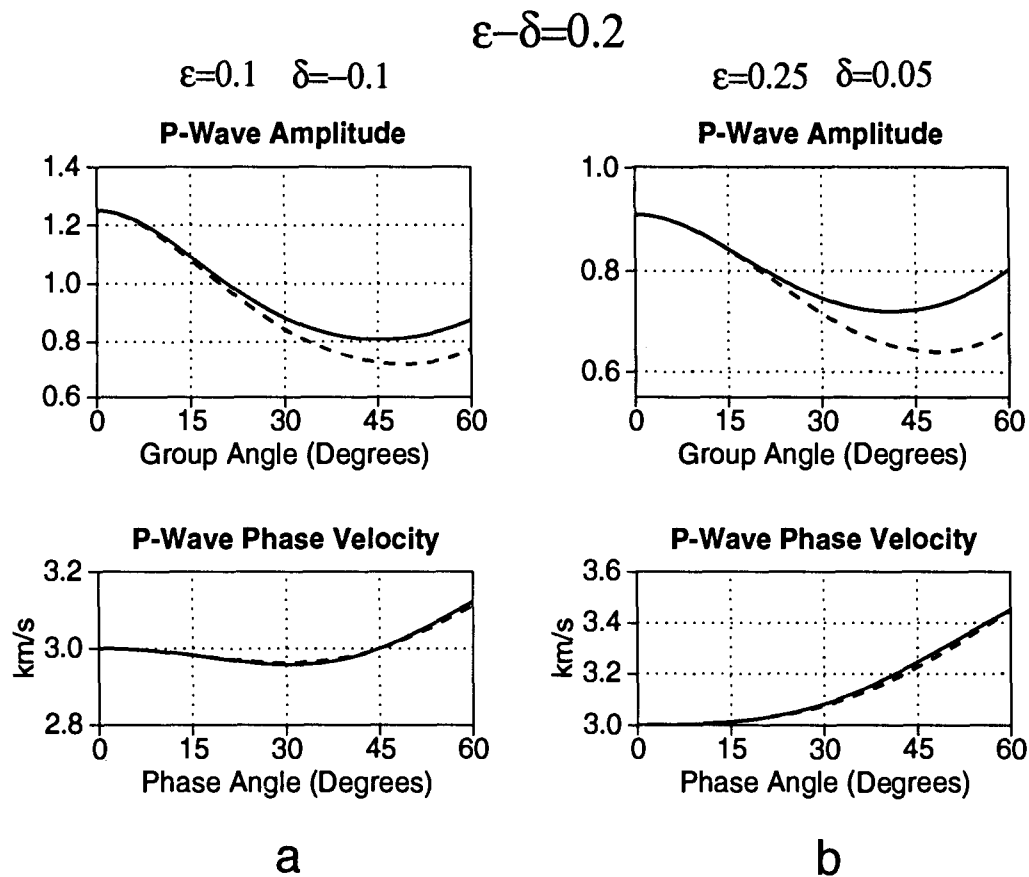Group Angle (Degrees)

P-Wave Phase Velocity

km/s

Phase Angle (Degrees)

b

FIG. 5. Normalized P-wave amplitude from a vertical force for models with ε − δ = 0.2.

is well-correlated with the character of the velocity variations (Figure 6). If the value of $\varepsilon = \delta$ is positive, both the velocity and the normalized amplitude increase away from vertical, but the amplitude variations in the angular range 0–40° remain mild, even for models with significant velocity anisotropy (Figure 6b). For the medium with $\varepsilon = \delta = 0.25$, the angular variation in the normalized amplitude (13% from 0 to 40°) is caused in part by the source term F_u because the P-wave polarization vector deviates somewhat from the source-receiver (group) direction. Elliptical anisotropy, however, may lead to a more significant change in the absolute value of the amplitude. For the same model with $\varepsilon = \delta = 0.25$, for example, the amplitudes near vertical are about 30% smaller than in the isotropic medium with the same V_{P0} and ρ.

To complete the analysis of P-wave radiation patterns, I examine amplitude signatures for models with negative $\varepsilon - \delta$ (Figure 7). In this (less typical) case, in agreement with the weak-anisotropy result [equation (8)], the anisotropy leads to an increase in the P-wave amplitude with angle. Note, that for models with $\varepsilon - \delta < 0$, the amplitude signature is much more controlled by the difference $\varepsilon - \delta$ than for models with positive $\varepsilon - \delta$. For both media in Figure 7, which have the same $\varepsilon - \delta = -0.1$ but different individual values of δ and ε, the increase in the normalized amplitude from 0 to 40° is almost the same ($\approx 25\%$).

The accuracy of the weak-anisotropy approximation turns out to be higher for elliptical anisotropy ($\varepsilon = \delta$) and models with negative $\varepsilon - \delta$ than for media with $\varepsilon - \delta > 0$. Even for ε and δ in the 20–25% range, the weak-anisotropy result in Figures 6 and 7 does not deviate much from the exact amplitude for incidence angles up to 40–45 degrees.

Radiation pattern versus reflection coefficient

How do the distortions of the P-wave radiation pattern compare with the influence of transverse isotropy on the reflection coefficient? Thomsen (1993) derived an approximation for the P-wave reflection coefficient in the limit of weak transverse isotropy, and small velocity and density contrasts at the reflector. Here, I give Thomsen's equation with a correction by Rüger ("P-wave reflections and azimuthal dependence of AVO in transversely isotropic media," Center for Wave Phenomena Project Review, CSM, 1995):

$$R(\theta) = R_{\text{isot}}(\theta) + R_{\text{anis}}(\theta), \qquad (11)$$

where $R_{\text{isot}}(\theta)$ is the reflection coefficient in the absence of anisotropy ($\varepsilon = 0$, $\delta = 0$), and

$$R_{\text{anis}}(\theta) = \frac{1}{2}(\delta_2 - \delta_1) \sin^2 \theta$$

$$+ \frac{1}{2}(\varepsilon_2 - \varepsilon_1) \sin^2 \theta \tan^2 \theta. \qquad (12)$$

Subscripts 1 and 2 refer to the media above and below the reflector, respectively. One of the convenient features of equations (11) and (12) is the separation of the "isotropic" and "anisotropic" parts of the reflection coefficient. Formula (12) is an improvement over Banik's (1987) approximation, which is limited to small incidence angles.

Unlike the radiation pattern, the reflection coefficient at normal incidence is not distorted by transverse isotropy if

the density and P-wave vertical velocity are the same in the isotropic and TI models. Note that the lowest-order angular correction to the reflection coefficient depends just on the change in δ across the reflector (no dependence on ε), while the lowest-order angular term in radiation pattern (8) contains the difference between ε and δ.

To compare the influence of transverse isotropy on the radiation pattern and on the reflection coefficient, we assume that the medium below the reflector is isotropic (e.g., the shale/sand AVO model discussed in Kim et al., 1993). Then

$$R_{\text{anis}}(\theta) = -\frac{1}{2}\delta_1 \sin^2 \theta - \frac{1}{2}\varepsilon_1 \sin^2 \theta \tan^2 \theta. \qquad (13)$$

For the two models shown in Figure 8, the importance of the propagation phenomena is quite different. If $\varepsilon = 0.1$ and $\delta = -0.1$ (Figure 8a), the anisotropy causes a 35% drop in the amplitude from 0 to 40°, while the anisotropy-induced angular variations in the reflection coefficient do not exceed 0.01. Hence, for a typical value of R_{isot} of about 0.1, transverse isotropy would make less than a 10% change in the total reflection coefficient. Thus, in this case the redistribution of energy above the reflector is likely to be a much more important factor in AVO than the influence of the anisotropy on the reflection coefficient.

In contrast, for the model in Figure 8b, the distortions of the radiation pattern in the 0–40° range are limited to 7% as compared with the absolute change in the anisotropic part of the reflection coefficient (R_{anis}) of about 0.05. For typical (small) values of R_{isot}, we can expect the distortions of the reflection coefficient to be the dominant effect of transverse isotropy on AVO for this model. Obviously, it is difficult to make a general comparison between the influence of anisotropy on wave propagation and reflection coefficients. The angular variations in the reflection coefficient depend on the difference in the anisotropic parameters across the reflector, while the radiation pattern is determined entirely by the properties of the incidence medium. Also, the influence of anisotropy on the reflection coefficient depends on the impedance contrast, i.e., it is more pronounced for weak reflectors. However, it is clear that the two phenomena are often of the same order of magnitude.

More examples of P-wave reflection coefficients in transversely isotropic media are provided in Kim et al. (1993) and Blangy (1994). Kim et al. (1993) studied a shale/sand boundary under the assumption that only the shale (the medium above the reflector) is anisotropic. For moderate values of ε and δ in the shale, the difference between the isotropic and anisotropic reflection coefficients at an incidence angle of 40° is usually limited by ± 0.05. In one of the typical cases considered in Kim et al. (1993) (Class 2 gas sands), this difference amounts to a 30–35% error in the reflection coefficient, which is comparable to the distortions of the radiation pattern we have discussed above.

In isotropic AVO analysis, the presence of gas is often identified by an increase in the absolute value of the P-wave reflection coefficient with angle. Kim et al. (1993) concluded that transverse isotropy above the reflector usually enhances this behavior by further increasing the absolute value of the reflection coefficient away from vertical. Our analysis shows that the propagation phenomena in typical TI media (with $\varepsilon - \delta > 0$) above the reflector may lead to a decrease in the
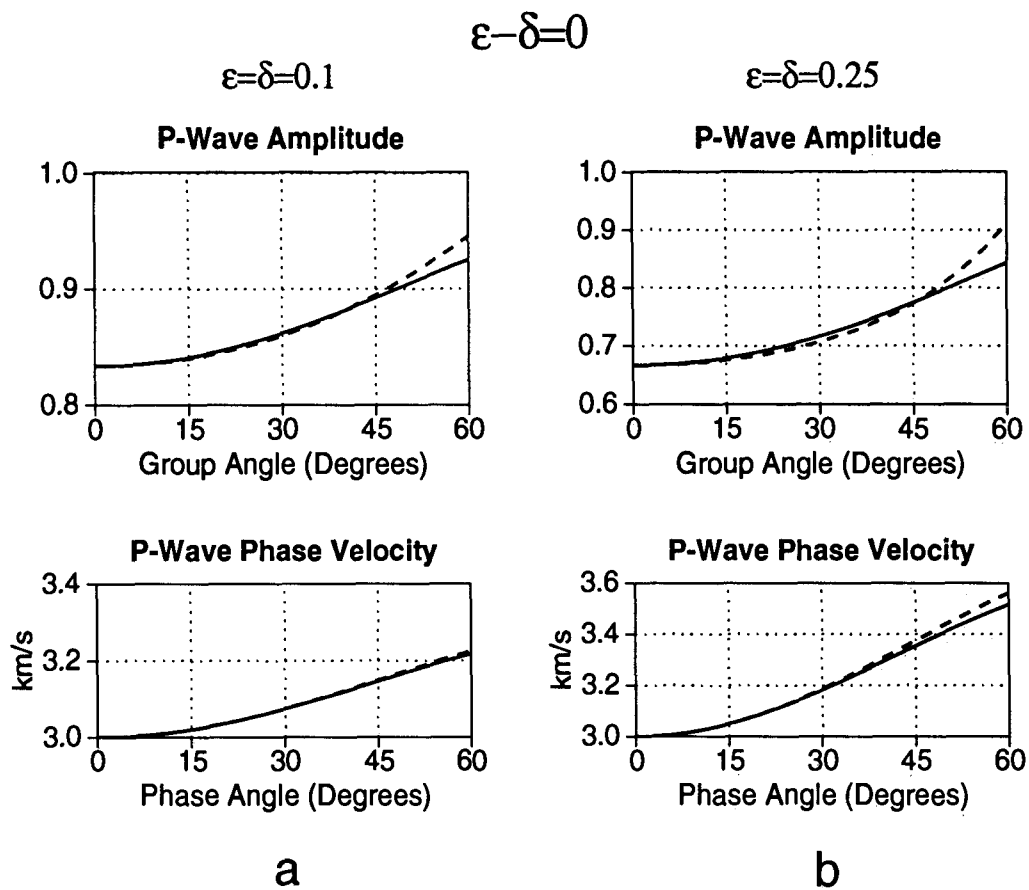
ε–δ=0

ε=δ=0.1

P-Wave Amplitude

Group Angle (Degrees)

P-Wave Phase Velocity

Phase Angle (Degrees)

a

ε=δ=0.25

P-Wave Amplitude

Group Angle (Degrees)

P-Wave Phase Velocity

Phase Angle (Degrees)

b

Fig. 6. Normalized P-wave amplitude from a vertical force for models with $\varepsilon - \delta = 0$ (elliptical anisotropy).

ε–δ=–0.1

ε=0   δ=0.1

P-Wave Amplitude

Group Angle (Degrees)

P-Wave Phase Velocity

Phase Angle (Degrees)

a

ε=0.1   δ=0.2

P-Wave Amplitude

Group Angle (Degrees)

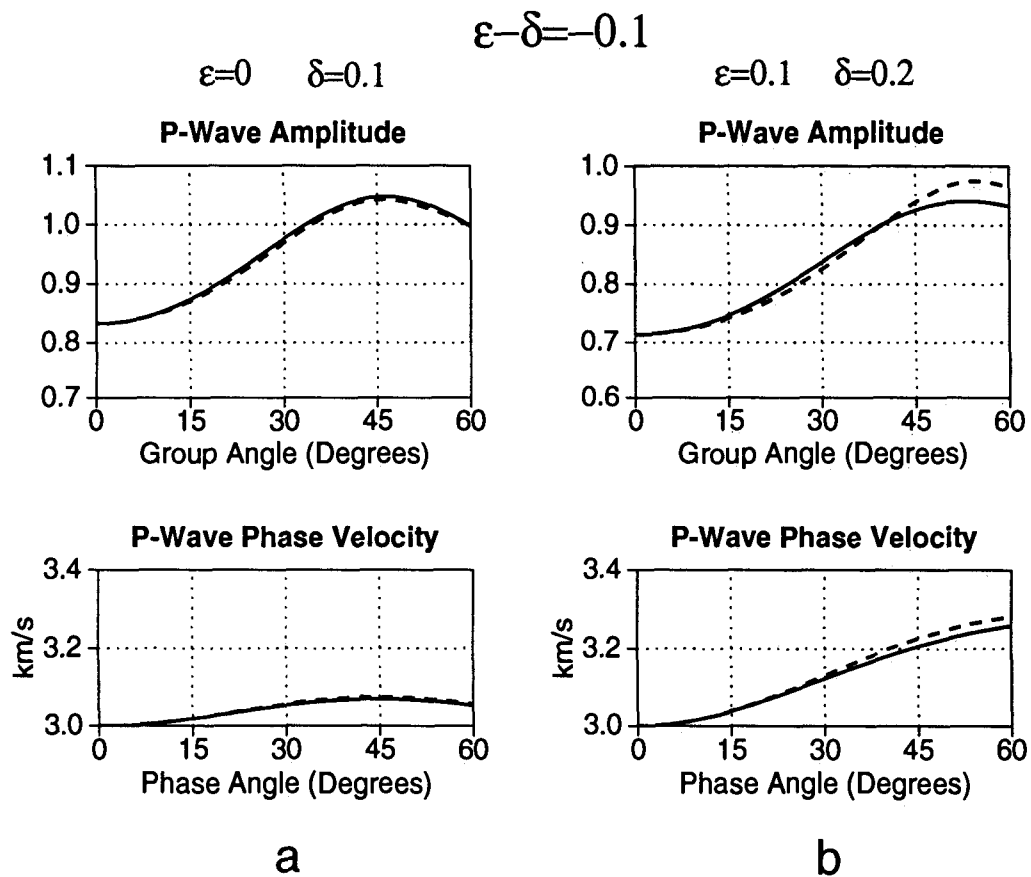**P-Wave Phase Velocity**

Phase Angle (Degrees)

b

Fig. 7. Normalized P-wave amplitude from a vertical force for models with $\varepsilon - \delta = -0.1$.

amplitude with angle and, therefore, reduce or reverse the influence of the anisotropy on the reflection coefficient. For "bright spots" with large normal-incidence reflection coefficients and a relatively slow increase in the absolute value of the reflection coefficient with angle [Class 3 sands from Kim et al. (1993)], amplitude distortions above the reflector may even reverse the sign of the AVO gradient!

SHEAR-WAVE RADIATION PATTERNS

SV-wave

The phase velocity of the SV-wave in transversely isotropic media is mostly determined by the effective parameter denoted in Tsvankin and Thomsen (1994) as σ:

$$\sigma = \frac{V_{P0}^2}{V_{S0}^2} (\varepsilon - \delta). \tag{14}$$

In the weak-anisotropy approximation, the SV-wave phase velocity is given by (Thomsen, 1986)

$$V_{SV}(\theta) = V_{S0}(1 + \sigma \sin^2 \theta \cos^2 \theta). \tag{15}$$

The terms "weak" or "strong" velocity anisotropy for the SV-wave refer mostly to the value of σ [equation (14)] rather

than to the individual values of ε and δ, although ε, δ, and the V_{P0}/V_{S0} ratio do have some separate influence on the SV-wave velocity if σ is not small.

Equation (15) can be obtained from the P-wave phase velocity [equation (5)] by replacing V_{P0} with V_{S0}, δ with σ, and setting $\varepsilon = 0$. Since the radiation pattern in the weak-anisotropy approximation (4) is a function of phase velocity (except for the source term F_u), the SV-wave radiation pattern can be derived from the P-wave formula (8) by making the same substitutions ($V_{P0} = V_{S0}$, $\delta = \sigma$, $\varepsilon = 0$):

$$U_{SV}(R, \theta) = \frac{F_u}{4\pi\rho V_{S0}^2 R} \frac{1 + 2\sigma \sin^2 2\theta + \sigma \sin^2 \theta}{1 + 2\sigma}. \tag{16}$$

The weak-anisotropy formula is exact in the symmetry direction where the anisotropic correction factor is given by $1/(1 + 2\sigma)$. Note that $V_{S0} \sqrt{1 + 2\sigma}$ is the SV-wave NMO velocity from a horizontal reflector. Therefore, as for the P-wave, the SV-wave amplitude in the symmetry direction ($\theta = 0$) and the NMO velocity are controlled by the same expression; for the SV-wave, this expression is $1 + 2\sigma$.

In addition to maxima or minima at $\theta = 0$ and $\theta = 90°$, the SV-wave phase velocity function has an extremum near 45° (unless $\varepsilon = \delta$, in which case V_{SV} is constant). In the most

$\varepsilon=0.1 \quad \delta=-0.1$

Incident P-Wave Amplitude

$\varepsilon=0.2 \quad \delta=0.1$

Incident P-Wave Amplitude

Reflection Coefficient

Reflection Coefficient

a   b
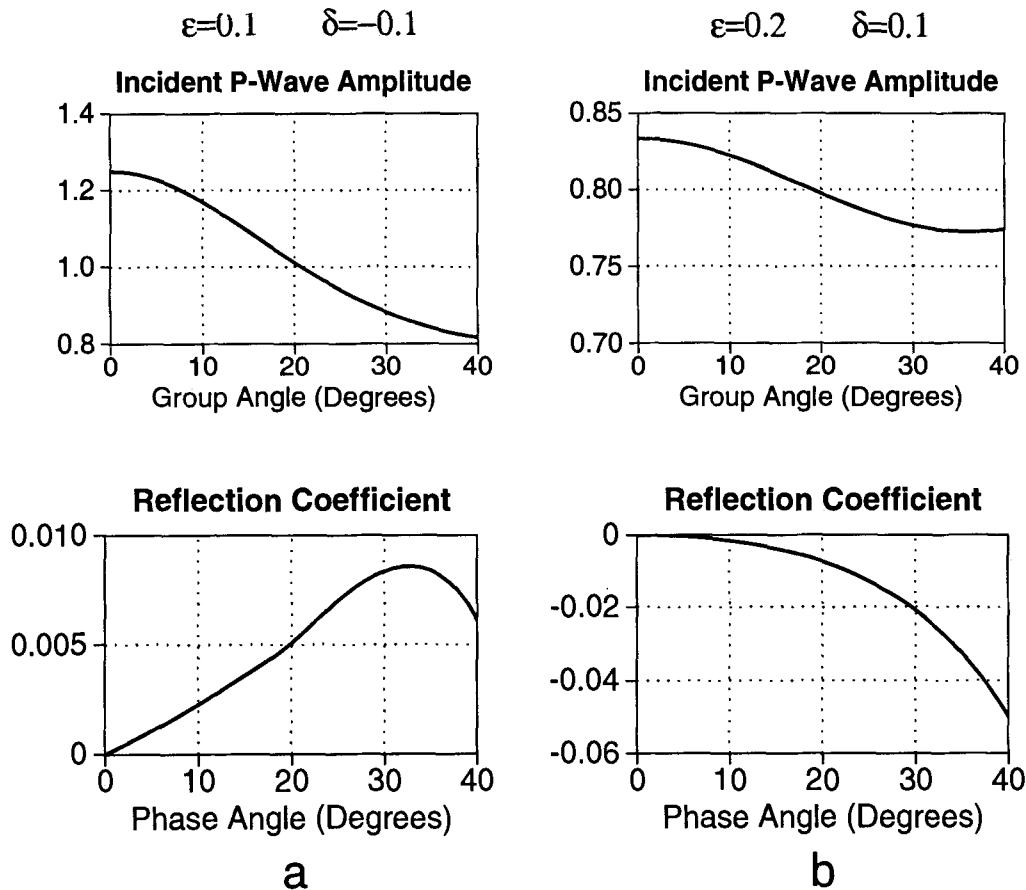
FIG. 8. Comparison of the influence of transverse isotropy on the P-wave radiation pattern (from a vertical force) and on the reflection coefficient. (Top) The exact far-field amplitude of the incident wave from equation (A-4) normalized by the amplitude in the corresponding isotropic medium with $\varepsilon = \delta = 0$. (Bottom) The angular variation in the reflection coefficient caused solely by the anisotropy [equation (13)]. It is assumed that the transversely isotropic models with ε and δ shown on the plot overlie an isotropic medium.

common case of positive σ ($\varepsilon > \delta$), the SV-wave phase velocity has a minimum at vertical incidence followed by a maximum near 45° (exactly the same as the P-wave velocity for $\varepsilon = 0$, $\delta > 0$). As shown by formula (16) and the analysis in the previous section, this leads to an increase in the incident wave amplitude with angle. An important difference, however, is that σ is often much bigger than δ because of the contribution of the squared velocity ratio. It is also noteworthy that the polarization direction and, consequently, the term F_u is often much more distorted by transverse isotropy for the SV-wave than for the P-wave (Tsvankin and Chesnokov, 1990a).

Figure 9 shows the SV-wave amplitude for the same olivine model as in Figure 2, which has a positive value of $\varepsilon - \delta$, thus yielding $\sigma > 0$. The SV-wave velocity anisotropy (i.e., the maximum variation in velocity) for this model is only about 4.3%. Nevertheless, the focusing of energy near the velocity maximum causes a pronounced increase in the normalized SV-wave amplitude near the 45° angle.

The stationary-phase solution (solid curve) remains close to the exact amplitude (dotted curve) within the whole angular range shown in Figure 9 [the area near the symmetry (vertical) axis, not shown on the plot, corresponds to the minimum of the radiation pattern where the amplitude goes to zero]. This verifies the accuracy of the stationary-phase result [equation (A-4)] in describing far-field SV amplitudes.

Normalized SV-Wave Amplitude

Group Angle (Degrees)

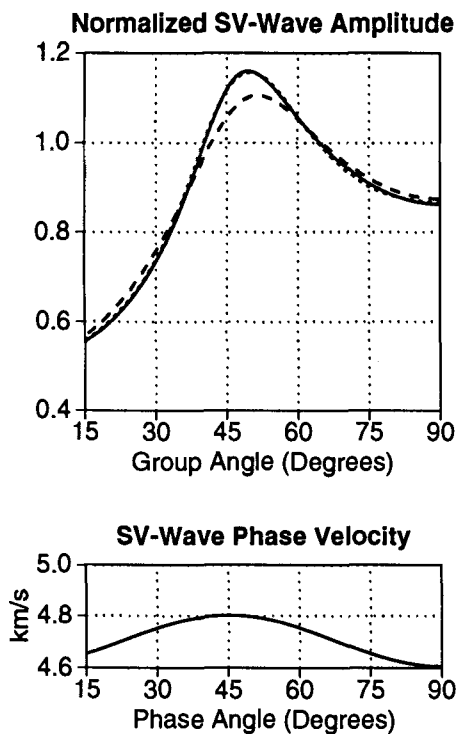## SV-Wave Phase Velocity

Phase Angle (Degrees)

Fig. 9. SV-wave amplitude from a vertical force in transversely isotropic olivine (model from Figure 2, $\sigma = 0.168$). The dotted curve is the exact result obtained by evaluating Fourier-Bessel integrals; the solid curve is the stationary-phase solution (A-4); and the dashed curve is the weak-anisotropy approximation (16). All three curves are normalized by the radiation pattern in the corresponding isotropic medium ($\varepsilon = 0$, $\delta = 0$).

Although the coefficient σ is not small ($\sigma = 0.168$), the error of the weak anisotropy approximation (16) for this model does not exceed 6%.

Figures 10 and 11 show the normalized SV-wave radiation patterns from a horizontal force for a suite of models with σ varying from zero (elliptical anisotropy) to 0.45. The amplitudes were calculated using the stationary-phase solution [equation (A-4)] (solid curve) and the weak-anisotropy approximation (16) (dashed curve).

Elliptical anisotropy ($\sigma = 0$, Figure 10a) seems to be equivalent to isotropy for the SV-wave because the SV-wave phase and group velocities do not change with angle. However, even in this case the SV radiation pattern deviates from the isotropic one because of the influence of the source term F_u, i.e., as a result of the polarization anomalies. In the example with $\varepsilon = \delta = 0.2$ shown in Figure 10a, the anisotropy tilts the SV-wave polarization vector towards vertical, thus reducing the amplitude generated by a horizontal force. It is interesting that for the SV-wave from a vertical force in the same model, the influence of the anisotropy leads to higher amplitudes. This explains the distortions of the SV-wave radiation pattern found by Ben-Menahem et al. (1991) and Gajewski (1993) for the elliptically anisotropic model of "Wills Point shale," which has $\varepsilon = \delta = 0.37$. It should be mentioned that the original elastic constants of Wills Point shale, experimentally determined in Robertson and Corrigan (1983), did not yield elliptical anisotropy; Ben-Menahem et al. (1991) adjusted the elastic coefficients reported in Robertson and Corrigan (1983) to make the model elliptical. On the whole, for elliptical anisotropy the SV-wave amplitude distortions in the range 0–40° are mild unless the value of $\varepsilon = \delta$ is unusually large.

Although the medium with $\varepsilon - \delta = 0.05$ (Figure 10b) seems to be close to elliptical and the maximum velocity variation is just about 3.5%, the SV-wave amplitude signature is distinctly different from the one for elliptical anisotropy. The value of $\sigma = 0.15$ is sufficient to make the normalized amplitude increase by 34.5% from 0 to 40°.

For larger σ, the velocity minimum at vertical and the maximum near 45° become sharper, making the SV-wave amplitude anomaly much more pronounced (Figure 11). For the medium with $\sigma = 0.3$ (Figure 11a), the increase in the normalized amplitude between 0 and 40° reaches 85%, while the maximum SV-wave velocity variation is only about 6.3%.

These results are in good agreement with SV-wave focusing phenomena described in Tsvankin and Chesnokov (1990a) and Gajewski (1993). Here, the numerical results are supported by a consistent analytic treatment of the amplitude anomalies in terms of σ. It should be mentioned, however, that for models with relatively large σ (like the ones in Figure 11), the SV radiation pattern becomes more dependent on the individual values of ε, δ, and V_{P0}/V_{S0}.

With a further increase in σ, the Gaussian curvature of the slowness surface at the velocity maximum decreases, eventually leading to a parabolic point where the curvature goes to zero [see a discussion in Gajewski (1993)]. At parabolic points, the stationary-phase solution (A-4) is invalid since its denominator goes to zero and the amplitude becomes infinite. This deficiency is common for all high-frequency ray-theory solutions, including those presented in Ben-Menahem

et al. (1991) and Gajewski (1993). Note that the numerical method based on evaluation of Fourier-Bessel integrals (Tsvankin and Chesnokov, 1990a) remains valid even at parabolic points.

For even larger σ, SV-wavefronts exhibit cusps centered near phase-velocity maxima. The distribution of energy within the cusps is more complicated than just a single amplitude maximum as in the models considered above, and may not be adequately described by the stationary-phase expression (A-4).

As demonstrated in Figures 10 and 11, the error of the weak-anisotropy approximation (16) in the angular range 0–$40°$ does not exceed 10% if $\sigma < 0.2 - 0.25$. In a more limited range, 0–$30°$, the weak-anisotropy result remains close to the exact amplitude for much higher values of σ (see the model with $\sigma = 0.45$). However, for $\sigma = 0.45$ the weak-anisotropy approximation breaks down completely for group angles over $40°$, mostly because of the inaccuracy in the weak-anisotropy expression for the group angle.

Large-magnitude distortions of SV amplitudes, even in models with moderate velocity anisotropy, mean that AVO for SV-waves will be impossible to carry out without an elaborate correction for propagation phenomena. Such correction, however, will require accurate estimates of the anisotropic coefficients, especially the effective parameter σ.

SH-wave

The SH-wave slowness surface in a homogeneous transversely isotropic medium is elliptical, and the phase velocity is given (exactly) by

$$V_{SH}(\theta) = V_{S0}\sqrt{1 + 2\gamma \sin^2 \theta},$$

where γ is as defined in equation (3).

As discussed above, for elliptical anisotropy the far-field solution [equation (A-4)] reduces to a concise formula without using the weak-anisotropy approximation. For the SH-wave, equation (A-4) yields

$$U_{SH}(R, \psi) = \frac{F_u}{4\pi\rho V_{S0}^2 R} \frac{1}{\sqrt{(1 + 2\gamma)(1 + 2\gamma \cos^2 \psi)}},$$

(17)

where ψ is the group angle. In any plane containing the symmetry axis, the source term F_u is constant: $F_u = F_2$, where F_2 is the force component perpendicular to the incidence plane. Equation (17) coincides with a formula obtained by Ben-Menahem (1990) in a different way. Again, as for the P- and SV-waves, the contribution of the anisotropy to the SH amplitude in the symmetry direction and to the NMO velocity is determined by the same expression $(1 + 2\gamma)$.

The SH-wave radiation pattern [equation (17)] is practically identical to the P-wave pattern for elliptical anisotropy [$\varepsilon = \delta$, equation (10)], with V_{P0} and δ replaced by V_{S0} and γ, respectively. The only difference between the two expressions is that the source term F_2 for the SH-wave is constant because the polarization direction does not change with incidence angle.

For weak SH-wave velocity anisotropy ($\gamma \ll 1$), equation (17) reduces to

$$U_{SH}(R, \psi) = \frac{F_2}{4\pi\rho V_{S0}^2 R} \frac{1 + \gamma \sin^2 \psi}{1 + 2\gamma}.$$

(18)

Again, expression (18) has the same form as the weak-anisotropy approximation for the P-wave [equation (8)] in elliptically anisotropic media.

The parameter γ is usually positive (Thomsen, 1986); γ is always positive for transverse isotropy resulting from thin bedding of isotropic layers. If $\gamma > 0$, the defocusing of energy at vertical incidence leads to an increase in the SH-wave amplitude with angle. However, as for the P-wave in elliptically anisotropic media, distortions of SH radiation patterns are relatively mild. For instance, even for a large γ of 0.3 (yielding about 26% SH-wave velocity anisotropy), the amplitude increase from 0 to $45°$ is limited to just 11%. The absolute change in the amplitude caused by the anisotropy is much more pronounced, but this is a different issue.

We have discussed the angular distribution of amplitude for a fixed source-receiver distance ($R = $ const). It is also interesting to examine the SH-wave amplitude along the wavefront at a fixed time t. Then equation (17) becomes

$$U_{SH}(t, \psi) = \frac{F_2}{4\pi\rho V_{S0}^2(V_{S0}t)(1 + 2\gamma)}.$$

(19)

Equation (19) shows that the SH-wave amplitude along the wavefront is constant (as in isotropic media), although the wavefront is elliptical rather than spherical; the influence of anisotropy reduces to the scaling factor $1 + 2\gamma$. Note that this conclusion is not quite true for the P-wave in elliptically anisotropic media: the source term F_u and, consequently, the P-wave amplitude variation along the wavefront is influenced by the anisotropy even in this case.

The conclusion that the influence of transverse isotropy on the shape of SV radiation patterns is much more significant than that on SH patterns is in good agreement with experimental results by Robertson and Corrigan (1983), who measured shear-wave radiation patterns in anisotropic shales with positive σ. They have found a strong focusing of energy of the SV-wave near the $45°$ incidence angle, while the SH radiation pattern did not deviate much from the isotropic one, despite significant velocity anisotropy for the SH-wave.

DISCUSSION AND CONCLUSIONS

Since conventional methods used to compensate for propagation phenomena in AVO analysis are based on the assumption of isotropy, the influence of anisotropy on wave propagation to and from a reflector may have a direct influence on the character of AVO anomalies. These propagation phenomena may be of equal or greater importance to AVO analysis than the influence of anisotropy on the reflection coefficient, especially for strong reflectors or small differences in the anisotropic coefficients across the reflector. If not properly corrected for, the anisotropic directivity factor may lead to a change or even a sign reversal in the AVO gradient that is conventionally used for hydrocarbon detection.

Here, the relation between P- and S-wave radiation patterns from a point force and AVO response has been analyzed for transversely isotropic models. A concise ana-

$\sigma=0$ $(\epsilon=\delta=0.2)$ $\sigma=0.15$ $(\epsilon=0.1,\ \delta=0.05)$
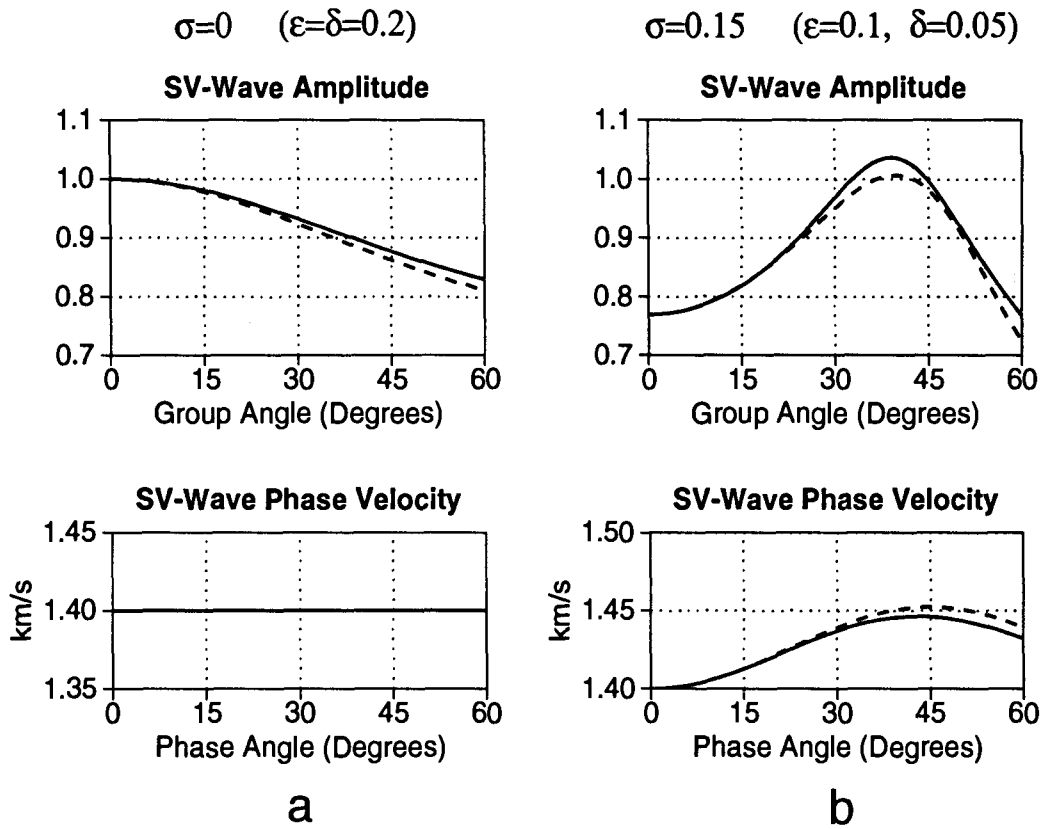

FIG. 10. SV-wave amplitude from a horizontal force. The solid curve is the stationary-phase solution (A-4); the dashed curve is the weak-anisotropy approximation (16). The amplitude curves are normalized by the radiation pattern in the corresponding isotropic model ($\epsilon = 0$, $\delta = 0$). The plots at the bottom show the exact phase velocity (solid curve) and its weak-anisotropy approximation (15) (dashed curve).

$\sigma=0.3$ $(\epsilon=0.15,\ \delta=0.05)$ $\sigma=0.45$ $(\epsilon=0.2,\ \delta=0.05)$

FIG. 11. Normalized SV-wave amplitude from a horizontal force.

lytic solution, obtained in the weak-anisotropy approximation, relates the angular dependence of body-wave amplitudes to the anisotropic parameters ε, δ (for the P-wave), σ (SV-wave), and γ (SH-wave). Combined with the Thomsen's (1993) approximation for reflection coefficients in transversely isotropic media, this solution provides a framework for a comprehensive qualitative analysis of the influence of transverse isotropy on AVO. All analytic expressions in this paper are derived as a function of the phase or group angles with respect to the symmetry axis and, therefore, can be easily applied not only to VTI media, but also to transverse isotropy with any symmetry-axis orientation.

The character of the P-wave angular amplitude variations in the range of angles commonly used in AVO analysis (0–40°) is controlled mostly by the difference between the anisotropies ε and δ, and is practically independent of the shear-wave vertical velocity V_{S0}. For models with $\varepsilon - \delta > 0$, believed to be typical for subsurface formations, transverse isotropy may cause the P-wave amplitude to drop by 30% or more over the first 40° from vertical. If the difference $\varepsilon - \delta$ is positive, the influence of the anisotropy becomes stronger with increasing $\varepsilon - \delta$ and, for fixed $\varepsilon - \delta$, with *decreasing* values of ε and δ. Thus, there is no simple relation between the strength of the velocity anisotropy and the amplitude anomalies.

For elliptical anisotropy ($\varepsilon = \delta$), the distortions of the angular amplitude dependence are well-correlated with the velocity variations. For positive $\varepsilon = \delta$, the anisotropy leads to an increase in amplitude with angle, but these distortions in the 0–40° angular range are mild, even for models with significant velocity anisotropy. Thus, application of the elliptical-anisotropy approximation ($\varepsilon = \delta$) to P-wave amplitudes may lead to unacceptable errors even if the medium is relatively close to elliptical.

The weak-anisotropy approximation for P-wave radiation (8) is more accurate for models with $\varepsilon \leq \delta$ than for media with positive $\varepsilon - \delta$. If $\varepsilon - \delta > 0$, the weak-anisotropy result tends to overstate the angular amplitude variations caused by the anisotropy, with the error becoming higher for larger $\varepsilon - \delta$. For models with $0 < \varepsilon - \delta < 0.2$ (believed to be most typical), the accuracy of the weak-anisotropy approximation is sufficiently high. For example, the difference between the weak-anisotropy and exact amplitudes in the angular range 0–40° remains within 10%, even if ε reaches 0.25. The main importance of the weak-anisotropy formula, however, is in providing a convenient tool for qualitative amplitude estimates for a wide range of transversely isotropic models.

The distortions of the SV-wave radiation pattern in typical TI models are much more significant than those for the P-wave. The influence of transverse isotropy on SV-wave amplitudes is determined mostly by the effective parameter σ introduced in Tsvankin and Thomsen (1994). For the SH-wave, the anisotropy is elliptical, and the distortions in the angular amplitude dependence are relatively mild, even for substantial velocity variations. Moreover, the SH-wave amplitude along the wavefront (rather than at a constant source-receiver distance) in any plane containing the symmetry axis does not change at all. These results for shear waves agree with those in the case study by Robertson and Corrigan (1983).

Here, I have examined the influence of radiation patterns on AVO only for VTI models. As shown in Tsvankin and Chesnokov (1990a), azimuthal anisotropy may significantly reinforce distortions of radiation patterns, even within symmetry planes (e.g., in orthorhombic media). Also, body-wave amplitudes may be significantly disturbed by shear-wave point singularities (Crampin, 1991).

An approximate correction for anisotropic propagation phenomena in simple models such as the one considered here can be made by using asymptotic expressions for radiation patterns like those discussed in this paper or presented in Gajewski (1993). However, the redistribution of energy along the wavefront may occur not only in the source layer but also in any anisotropic layer between the reflector and the surface. In this case, it is necessary to apply numerical methods capable of allowing for anisotropy in wave propagation through layered media. Anisotropic propagation phenomena should also be included in any algorithm designed to use reflection coefficients to invert for the anisotropic parameters.

If the overburden is laterally homogeneous, it is possible to correct for the propagation effects by doing amplitude calibration at well locations (J. Castagna, pers. comm.). However, such a correction allows one to recover only lateral variations in the reflection coefficient unless it is possible to obtain the reflection coefficient itself from, say, rock properties measurements. And, of course, any lateral changes in the overburden will make this calibration inaccurate.

Still, the greatest challenge in correcting AVO signatures for anisotropy is to determine the anisotropic parameters with sufficient accuracy. The lowest-order correction to the reflection coefficient depends just on the value of δ above and below the reflector. For VTI media, δ can be determined in a straightforward way from the P-wave normal-moveout (NMO) velocity and the true vertical velocity, if well logs or check shots are available. However, an accurate correction for propagation phenomena requires knowledge not only of δ, but also of ε. If shear data are acquired, the parameter ε can be obtained from the NMO velocity of the SV-wave (or $P - SV$-wave) and the vertical velocity, provided δ has been determined. Also, Alkhalifah and Tsvankin ("Velocity analysis for transversely isotropic media," GEOPHYSICS this issue) show that in the presence of dipping reflectors, both ε and δ can be recovered from the dependence of the P-wave NMO velocity on the ray parameter, if the true vertical velocity is known.

ACKNOWLEDGMENTS

at the Center for Wave Phenomena, Colorado School of Mines, and by the United States Department of Energy, Grant Number DE-FG02-89ER14079 (this support does not constitute an endorsement by DOE of the views expressed in this paper).

REFERENCES

Aki, K., and Richards, P. G., 1980, Quantitative seismology: Theory and methods: Vol. 1, W. N. Freeman & Co.
Banik, N. C., 1984, Velocity anisotropy of shales and depth estimation in the North Sea Basin: Geophysics, 49, 1411–1419.
Banik, N. C., 1987, An effective parameter in transversely isotropic media: Geophysics, 52, 1654–1664.
Ben-Menahem, A., 1990, SH waves from point sources in anisotropic inhomogeneous media: Geophysics, 55, 488–491.
Ben-Menahem, A., Gibson Jr., R. L., and Sena, A. G., 1991, Green's tensor and radiation patterns of point sources in general anisotropic inhomogeneous elastic media: Geophys. J. Int., 107, 297–308.
Berryman, J. G., 1979, Long-wave elastic anisotropy in transversely isotropic media: Geophysics, 44, 896–917.
Blangy, J. P., 1994, AVO in transversely isotropic media—An overview: Geophysics, 59, 775–781.
Crampin, S., 1991, Effects of singularities on shear-wave propagation in sedimentary basins: Geophys. J. Int., 107, 531–543.
Duren, R. E., 1992, Range-equation weights for AVO: Geophysics, 57, 1203–1208.
Fryer, G. J., and Frazer, L. N., 1987, Seismic waves in stratified anisotropic media—II. Elastodynamic eigensolutions for some anisotropic systems: Geophys. J. Roy. Astr. Soc., 91, 73–101.
Gajewski, D., 1993, Radiation from point sources in general anisotropic media: Geophys. J. Int., 113, 299–317.
Graebner, M., 1992, Plane-wave reflection and transmission coeffi-

cients for a transversely isotropic solid: Geophysics, 57, 1512–1519.
Keith, C. M., and Crampin, S., 1977, Seismic body waves in anisotropic media: Reflection and refraction at a plane interface: Geophys. J. Roy. Astr. Soc., 49, 181–208.
Kim, K. Y., Wrolstad, K. H., and Aminzadeh, F., 1993, Effects of transverse isotropy on P-wave AVO for gas sands: Geophysics, 58, 883–888.
Martinez, R. D., 1993, Wave propagation effects on amplitude variation with offset measurements: A modeling study: Geophysics, 58, 534–543.
Robertson, J. D., and Corrigan, D., 1983, Radiation patterns of a shear-wave vibrator in a near-surface shale: Geophysics, 48, 19–26.
Samec, P., and Blangy, J. P., 1992, Viscoelastic attenuation, anisotropy, and AVO: Geophysics, 57, 441–450.
Sams, M. S., Worthington, M. H., King, M. S., and Shams Khanshir, M., 1993, A comparison of laboratory and field measurements of P-wave anisotropy: Geophys. Prosp., 41, 189–206.
Thomsen, L., 1986, Weak elastic anisotropy: Geophysics, 51, 1954–1966.
———— 1993, Weak anisotropic reflections: Offset dependent reflectivity, Castagna and Backus, Eds.: Soc. Expl. Geophys., 103–114.
Tsvankin, I., and Chesnokov, E., 1990a, Synthesis of body-wave seismograms from point sources in anisotropic media: J. Geophys. Res., 95(B7), 11 317–11 331.
———— 1990b, Synthetic waveforms and polarizations at the free surface of an anisotropic halfspace: Geophys. J. Int., 101, 497–505.
Tsvankin, I., and Thomsen, L., 1994, Nonhyperbolic reflection moveout in anisotropic media: Geophysics, 59, 1290–1304.
White, J. E., Martineau-Nicoletis, L., and Monash, C., 1983, Measured anisotropy in Pierre shale: Geophys. Prosp., 31, 709–725.
Wright, J., 1987, The effects of transverse isotropy on reflection amplitude vs offset: Geophysics, 52, 564–567.

APPENDIX

WEAK-ANISOTROPY APPROXIMATION FOR RADIATION PATTERNS IN TRANSVERSELY ISOTROPIC MEDIA

In Tsvankin and Chesnokov (1990a), point-source radiation in homogeneous arbitrarily anisotropic media was decomposed into a Weyl-type integral over plane waves. The displacement (in the frequency domain) from a point force located at the origin of a Cartesian coordinate system $[x_1, x_2, x_3]$ was shown to be

$$U = \frac{i\omega}{4\pi^2} \sum_{\nu=1}^{3}$$

$$\times \int_{-\infty}^{+\infty} \int_{-\infty}^{+\infty} U_{p\ell} \, e^{-i\omega(m_1 x_1 + m_2 x_2 + m_{3\nu} x_3)} \, dm_1 \, dm_2, \quad (A\text{-}1)$$

with the plane-wave displacement $U_{p\ell}$ given by the residual

$$U_{p\ell} = Res\left[\frac{1}{D(m_3)} G^{ad} F\right]_{m_{3\nu}}. \quad (A\text{-}2)$$

The summation over ν corresponds to three possible wave types; m is the slowness vector; $G_{ik} = c_{ijk\ell} m_j m_\ell - \rho\delta_{ik}$ is the Christoffel matrix; G^{ad} is the adjoint matrix of G; $m_{3\nu}$ (the vertical slownesses of the plane waves) are roots of $D(m_3) = detG = 0$; and F is the point-force vector. To obtain the solution in the time domain, equation (A-1) should be multiplied with the frequency spectrum of the source pulse and substituted into the inverse Fourier transform.

It is convenient to represent equation (A-1) in polar coordinates $(m_1 = m_0 \cos \phi, m_2 = m_0 \sin \phi)$:

$$U = \frac{i\omega}{(2\pi)^2} \sum_{\nu=1}^{3}$$

$$\times \int_0^{+\infty} \int_0^{2\pi} U_{p\ell} \, e^{-i\omega(m_0 r \cos (\phi-\alpha)+m_{3\nu}z)} \, m_0 \, dm_0 \, d\phi, \quad (A\text{-}3)$$

$x_1 = r \cos \alpha, x_2 = r \sin \alpha, x_3 = z.$

In Tsvankin and Chesnokov (1990a), the radiation pattern was derived from equation (A-3) by means of the stationary-phase approximation which is valid in the far-field. For the special case of transversely isotropic media, the stationary-phase point lies in the incidence plane $\phi = \alpha$, and the phase velocity depends only on the angle with the vertical (symmetry) axis. Then the general stationary-phase solution for the amplitude of the νth wave (for brevity, henceforth I omit the superscript ν) given in Tsvankin and Chesnokov (1990a) becomes

$$|U| = \frac{|U_{p\ell}|}{2\pi V} \frac{\sin \theta \left(\dfrac{\cos \theta}{V} + \dfrac{d(1/V)}{d\theta} \sin \theta\right)}{\sqrt{\dfrac{r \sin \theta}{V} \dfrac{d^2\Phi}{d\theta^2}}}, \quad (A\text{-}4)$$

$$\frac{d^2\Phi}{d\theta^2} = (r \sin \theta + z \cos \theta)\left[\frac{1}{V} - \frac{d^2(1/V)}{d\theta^2}\right.$$

$$\left. + \frac{2}{V}\left(\frac{r \cos \theta - z \sin \theta}{r \sin \theta + z \cos \theta}\right)^2\right], \qquad (A-5)$$

where $\Phi = -m_0 r - m_{3v} z$ is the frequency-independent part of the phase function in the incidence plane [see equation (A-3)], θ is the phase angle measured from the vertical (z) axis, and V is the phase velocity. Expression (A-4) should be evaluated at the phase angle θ, corresponding to a given ray (group velocity) angle ψ determined by the receiver position (tan $\psi = r/z$).

I will now transform the exact far-field solution for transverse isotropy (A-4) into a much simpler weak-anisotropy approximation. The derivation is given for the P-wave only; the radiation patterns of S-waves are obtained in a similar way.

In the following, it is assumed that the source and receiver are located in the $[x_1, x_3]$ plane. In this case, at the stationary-phase point $\phi = \alpha = 0$. It is convenient to represent $|U_{p\ell}|$ in equation (A-2) as an explicit function of the P-wave slowness vector. The nonzero components of the Christoffel matrix in the plane $[x_1, x_3]$ are

$$G_{11} = c_{11}m_0^2 + c_{44}m_3^2 - \rho, \qquad (A-6)$$

$$G_{22} = c_{66}m_0^2 + c_{44}m_3^2 - \rho, \qquad (A-7)$$

$$G_{33} = c_{44}m_0^2 + c_{33}m_3^2 - \rho, \qquad (A-8)$$

$$G_{13} = G_{31} = m_0 m_3 (c_{13} + c_{44}). \qquad (A-9)$$

The determinant of G is

$$D = detG = G_{22}(G_{11}G_{33} - G_{13}^2).$$

The vertical slownesses of the P- and SV-waves are the roots of the polynomial $G_{11}G_{33} - G_{13}^2$, while the solutions of $G_{22} = 0$ give the vertical slownesses for the SH-wave. Since the P-wave displacement vector lies in the $[x_1, x_3]$ plane, formula (A-2) for the P-wave yields

$$U_{p\ell 1} = H(F_1 G_{33} - F_3 G_{13}), \qquad (A-10)$$

$$U_{p\ell 3} = H(F_3 G_{11} - F_1 G_{13}), \qquad (A-11)$$

with

$$H = \frac{m_3 - m_{3P}}{detG}\bigg|_{m_{3P}} = \frac{1}{2c_{33}c_{44}m_{3P}(m_{3P}^2 - m_{3SV}^2)}, \qquad (A-12)$$

m_{3P} and m_{3SV} are the vertical slownesses of the P- and SV-waves for a fixed m_0. m_{3SV} is given by

$$m_{3SV}^2 = \frac{(c_{11}m_0^2 - \rho)(c_{44}m_0^2 - \rho)}{c_{33}c_{44}m_{3P}^2}. \qquad (A-13)$$

Taking into account that for m_{3P}, the expression $G_{11}G_{33} - G_{13}^2 = 0$, we find from equations (A-10) and (A-11) that

$$|U_{p\ell}| = HF_u(G_{11} + G_{33}), \qquad (A-14)$$

where F_u is the projection of the force on the plane-wave displacement vector $U_{p\ell}$.

Substituting H from equations (A-12) and (A-13), G_{11} from equation (A-6) and G_{33} from equation (A-8) into equation (A-14) yields

$$|U_{p\ell}| = \frac{F_u m_{3P}}{2} \frac{m_0^2(c_{11} + c_{44}) + m_{3P}^2(c_{33} + c_{44}) - 2\rho}{m_{3P}^4 c_{33} c_{44} - (c_{11}m_0^2 - \rho)(c_{44}m_0^2 - \rho)}. \qquad (A-15)$$

Equation (A-15) is valid for general transverse isotropy. At this point, we substitute $m_0 = \sin \theta/V$, $m_{3P} = \cos \theta/V$ and introduce the weak-anisotropy approximation for the P-wave phase velocity (Thomsen, 1986)

$$V_P(\theta) = V_{P0}(1 + \delta \sin^2 \theta \cos^2 \theta + \varepsilon \sin^4 \theta). \qquad (A-16)$$

Formula (A-16) along with the expressions for ε and δ [equations (1), (2) of the main text] can be used to find the weak-anisotropy approximation for equation (A-15). Linearization in ε and δ, after tedious but straightforward algebra, gives

$$|U_{p\ell}| = \frac{F_u}{2V_P(\theta)\,\rho\,\cos\,\theta}$$

$$\times [1 + 2\sin^2\theta(\delta\cos 2\theta + 2\varepsilon\sin^2\theta)]. \qquad (A-17)$$

The next step is to obtain the weak-anisotropy approximation for $d^2\Phi/d\theta^2$, equation (A-5). Expressing r and z through the source-receiver distance R ($r = R \sin \psi, z = R \cos \psi$), we find

$$r \sin \theta + z \cos \theta = R \cos (\psi - \theta), \qquad (A-18)$$

and

$$\frac{r \cos \theta - z \sin \theta}{r \sin \theta + z \cos \theta} = \frac{\tan \psi - \tan \theta}{1 + \tan \psi \tan \theta}. \qquad (A-19)$$

The weak-anisotropy approximation for the P-wave group angle ψ is (Thomsen, 1986)

$$\tan \psi = \tan \theta [1 + 2\delta + 4(\varepsilon - \delta) \sin^2 \theta]. \qquad (A-20)$$

Substituting equations (A-18), (A-19), (A-20) along with the derivative of the phase-velocity function (A-16) into formula (A-5) and dropping the terms quadratic in ε and δ, we get

$$\frac{d^2\Phi}{d\theta^2} = \frac{R}{V}\left(1 + \frac{1}{V}\frac{d^2V}{d\theta^2}\right). \qquad (A-21)$$

Using the phase-velocity function [equation (A-16)] in the numerator of equation (A-4) yields

$$\frac{\cos \theta}{V} + \frac{d(1/V)}{d\theta} \sin \theta = \frac{\cos \theta}{V}$$

$$\times [1 - 2\sin^2\theta(\delta\cos 2\theta + 2\varepsilon\sin^2\theta)]. \qquad (A-22)$$

Finally, formulas (A-17), (A-21), and (A-22) are substituted into the original stationary-phase expression (A-4):

$$|\mathbf{U}| = \frac{F_u}{4\pi\rho V^2 R} \, \frac{1}{\sqrt{\dfrac{\sin\psi}{\sin\theta}\left(1 + \dfrac{1}{V}\dfrac{d^2 V}{d\theta^2}\right)}}. \quad \text{(A-23)}$$

Equation (A-23) can be fully linearized in the anisotropies ε and δ. However, expression (A-23) is a useful intermediate result because analogous derivations lead to the same formula for S-waves. Linearized expressions for each wave type (P, SV, SH) are discussed in the main text.